Original article

Marina Cabrini*, Sergio Lorenzi, Tommaso Pastore and Fabio Maria Bolzoni

Environmentally assisted cracking of pipeline steels in CO_2 containing environment at near-neutral pH

DOI 10.1515/corrrev-2017-0053
Received February 7, 2017; accepted May 11, 2017

Abstract: The paper summarizes the results obtained by authors concerning near-neutral stress corrosion cracking (SCC) phenomena on buried pipelines. Stress corrosion tests according to different methodologies and fatigue propagation tests were executed on traditional steel grades. Tests were performed also on specimens precorroded according to a procedure developed to produce localized attacks similar to those observed during failure analysis on pipelines, acting as preferential sites for crack nucleation. Electrochemical tests were carried out in order to evaluate the influence of environmental parameter on pit formation. The main role of continuous plastic deformations on near-neutral SCC is confirmed. The effect of pH, CO_2, and bicarbonate concentrations on pitting formation is discussed.

Keywords: buried pipelines; corrosion; EAC; NN-SCC; oil and gas; steel.

1 Introduction

The environmental assisted cracking (EAC) of buried pipelines are related to three types of phenomena: carbonate-bicarbonate stress corrosion cracking (CB-SCC), near-neutral stress corrosion cracking (NN-SCC) (Parkins, 2000), and hydrogen embrittlement (HE) (Punter et al., 1992; Baker Jr. & Fessler, 2008). The latter, i.e. HE cracking, occurs on high-strength steels under cathodic protection at level of excessive polarization, producing relevant atomic hydrogen evolution (Cabrini et al., 2000, 2011, 2015). CB-SCC and NN-SCC are mainly related to the presence of CO_2 and its dissociated species dissolved in the soil moisture, which wets the metallic surface in areas of coating breakdown and disbonding, respectively (Parkins & Fessler, 1978; Parkins et al., 1984, 1993).

The first public document that attributed a pipeline failure to CB-SCC was in March 1965. A 610-mm-diameter pipeline conveying natural gas ruptured near Natchitoches (Louisiana, USA), killing 17 people (Shipilov & May, 2006). Further investigations showed the typical intergranular morphology of CB-SCC cracking and proposed the mechanism of crack propagation based on the preferential active dissolution of crack tip, which is nowadays commonly accepted (Parkins et al., 1993). The variation of loading, due to the daily pressure fluctuations (Parkins & Fessler, 1978; Parkins et al., 1993), strains the crack tip and breaks the protective film that tends to form in concentrated carbonate-bicarbonate solutions, allowing crack propagation by active local dissolution (Manfredi & Otegui, 2002).

2 NN-SCC

In 1985–1986, TransCanada Pipeline published the first case of stress corrosion cracking (SCC) having transgranular morphology, well different to the typical one of CB-SCC, which occurred on a pipeline having disbonded coating (Delanty & O'Beirne, 1992; National Energy Board, 1996). The features were subsequently confirmed by using hydrostatic tests and systematic digs along the involved pipelines (National Energy Board, 1996; Parkins, 2000; Cheng & Niu, 2007). Cases of NN-SCC were then reported in Australia, Russia, Italy, United States, Iran, Iraq, Pakistan, etc. (Shipilov & May, 2006).

The NN-SCC was originally called low-pH SCC to outline that the pH of solution found under coating, in the

***Corresponding author: Marina Cabrini,** Department of Engineering and Applied Sciences, University of Bergamo, viale Marconi 5, Dalmine, Bergamo 24044, Italy, e-mail: marina.cabrini@unibg.it. http://orcid.org/0000-0003-3901-8657; and Consorzio INSTM, Via Giuseppe Giusti 9, Firenze 50121, Italy
Sergio Lorenzi and Tommaso Pastore: Department of Engineering and Applied Sciences, University of Bergamo, viale Marconi 5, Dalmine, Bergamo 24044, Italy; and Consorzio INSTM, Via Giuseppe Giusti 9, Firenze 50121, Italy
Fabio Maria Bolzoni: Politecnico di Milano, Chemistry, Materials, and Chemical Engineering Department "G. Natta", Via Mancinelli 7, Milano 20131, Italy

zones of cracking, was notably lower than the one typical of CB-SCC. Then, the name was changed into the more suitable "near-neutral SCC" because the pH never reaches truly acidic conditions. Furthermore, NN-SCC was named transgranular stress corrosion cracking (TG-SCC) by considering the different fracture morphologies with respect to the CB-SCC, which is also named intergranular stress corrosion cracking (IG-SCC).

NN-SCC is always associated with high levels of general corrosion. Cracks are usually filled by corrosion products, and they are located in colonies along the longitudinal direction of pipeline – with small cracks coalescence to form larger crack – having high length over depth ratio (Chen, 2016).

Transverse oriented cracking was also reported. A previous work of Bolzoni et al. (2000) describes a circumferential rupture on a buried flow-line of API 5L X52 steel that occurred after 30 years of service (Bolzoni et al., 2000). It was caused by the unstable movements of the ground, which generated tensile stress along the axis in correspondence with the pipeline constraint. The pipe was coated by means of bituminous layer, and impressed current cathodic protection was applied. Several cracks were noticed on the external surface – in area of severe general corrosion attack – with relevant corrosion products under the coating. The largest dimension was about 10-mm length and 0.1 ÷ 1-mm width. The cracks were grouped in colonies, with preferential nucleation sites in correspondence of localized attacks. No cracks were noticed either in zones with continuous adherent coating or in the presence of coating discontinuities. Figure 1 shows the metallographic section of secondary transgranular cracks in condition of severe plastic deformation. Deviation or crack growth stop in the presence of large inclusions of manganese sulfide can occur between ferrite/pearlite bands.

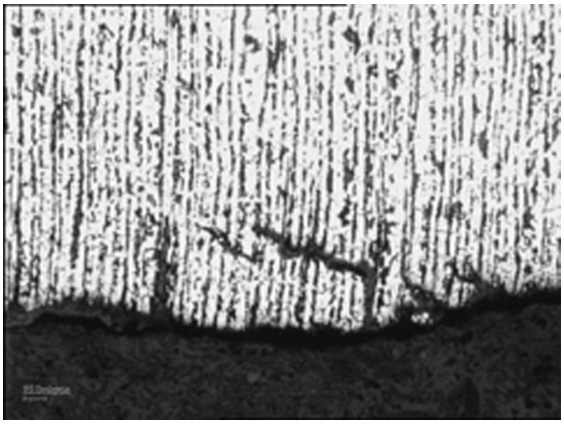

Figure 1: Metallographic section of secondary cracks.

The main environmental factors that distinguish NN-SCC from CB-SCC are pH and solution composition. NN-SCC occurs in solutions more diluted than ones critical for CB-SCC. Their low pH – that is, in the range 6.5–7, much lower than the dangerous range of 10–12 of CB-SCC – avoids relevant contents of carbonates and forms prevalent bicarbonate ions and undissociated species as Co_2 and carbonic acid (Beavers et al., 2000; National Energy Board, 1996).

The two forms of cracking are closely related to the biprotic nature of carbonic acid and the two buffer systems derived from it, affecting carbonic acid-bicarbonate and bicarbonate-carbonate pairs. The pH remains confined in a rather narrow range, and it cannot substantially modify unless one of the pairs disappears in favor of the other.

Further differences regard the position of ruptures and coating defects. Unlike CB-SCC, NN-SCC ruptures are not related to the distance from the gas compression stations, meaning that temperature plays a different role. Moreover, the cases occurred prevalently – but not exclusively – on pipelines coated with polyethylene belts, i.e. under linings that remain continuous even in the zones where coating detachment occurs, giving cavities into which the water can penetrate. The coating prevents the cathodic protection penetration toward the metal surface and avoids the alkalization caused by the cathodic oxygen reduction reaction. Such alkalization would immediately bring the pH outside the critical range for NN-SCC. Only in these circumstances that an almost neutral pH can be maintained (Parkins, 2000).

In spite of the numerous studies carried out on the matter, NN-SCC is not yet fully understood. The following work reports on results obtained in different research projects carried out to study NN-SCC by different techniques, for reproducing the phenomena on laboratory scale, evaluating the effect of environmental and loading parameters – pH, temperature, concentration of bicarbonate ions, and strain rate – and assessing cracking mechanisms. Constant load tests and constant displacement tests were carried out (Sinigaglia & Cabrini, 1997; Bolzoni et al., 1999). Slow strain rate tests on both uniaxial loaded specimens and three-point bending specimens, and linear elastic fracture mechanic (MFLE) tests on pre-cracked specimens were performed (Cabrini et al., 2010). The influence of surface finishing was also studied on both machined specimens and on pre-corroded specimens in order to simulate the localized attacks that promote NN-SCC (Cabrini et al., 2008a,b). Finally, the electrochemical behavior of pipeline steels was studied in order to assess the conditions that favor the localized attack initiation (Cabrini & Sinigaglia, 1996a,b).

3 Materials and methods

3.1 Stress corrosion tests

The tests were carried out on X52 and two X65 pipeline steel grades. Table 1 shows chemical compositions and mechanical properties. Metallographic examinations evidenced a ferritic-pearlitic structure with pearlite colonies and manganese sulfur inclusions oriented along the rolling direction.

The tests were carried out at 5.5 and 7 pH, in solutions based on the "NS4 solution" published by Parkins (2000) as the medium composition of soil moisture inducing cracking on TransCanada Pipeline. It contains 0.483 g/L $NaHCO_3$, 0.122 g/L KCl, 0.18 g/L $CaCl_2 \cdot 2H_2O$, 0.1 g/L $MgSO_4 \cdot 7H_2O$. Analytical grades Carlo Erba RPA (Italy) reagents were used. The pH, measured by means of a Amel (Italy) mod. 2335 digital pHmeter, was achieved by saturation with 1 atm pure CO_2 partial pressure (pH 5.5) and 5% CO_2/95% N_2 gas mixture (0.05 atm CO_2 partial pressure), respectively. The pH of the solution was measured just before and after tests in order to verify whether it was constant in a range of ±0.2 pH units. The solution was de-aerated for 12 h with nitrogen before CO_2 saturation.

Further tests were performed in solution modified by adding HCO_3^- ions to achieve pH 7 after saturation with 1 atm pure CO_2 partial pressure.

Tests were also carried out in 0.1 M Na_2SO_4 saturated with pure CO_2, with additions of H_2SO_4 or NaOH for modifying pH.

Tests were normally carried out at 25°C, with the exception of some tests conducted at 5°C, 50°C, and 70°C.

The following stress corrosion tests were performed:

- constant load tests
- constant deformation tests
- slow strain rate tests
- interrupted slow strain rate (ISSR) tests
- slow bending (SB) tests
- ripple loading tests

Constant load tests and constant deformation tests were performed in accordance with NACE TM01-77/90 and ASTM G30-90, respectively, at the free corrosion potential, which was usually about −0.520 V vs. NHE, and under 50 mV of anodic or cathodic polarization with respect to free corrosion potential E_{cor}. The exposure time was from 20 h to 6 months.

Slow strain rate tests were carried out in accordance with ISO 7539-7 on 3-mm-diameter cylindrical tensile specimens. The specimens were tested at strain rates in the range of 1.1×10^{-7} to 6.7×10^{-5} s^{-1}. SCC susceptibility was evaluated through the normalized reduction of area (NRA), that is, the ratio between the reduction of area obtained after the SSR tests in solution and values obtained in air, by calculating the embrittlement index (EI%) according to equation (1):

$$EI\% = (1 - NRA) \cdot 100 \quad (1)$$

The presence of brittle areas on the fracture surface and secondary cracks was also assessed.

ISSR tests were carried out in accordance with the same methodology of SSR tests. During ISSR tests, the specimen was initially loaded at an elongation rate of 10^{-5} s^{-1} to exceed the maximum load. The increase of elongation was interrupted when the load was reduced by 5% with respect to the maximum load. Afterwards, the specimen was left at constant elongation for 1 week.

Figure 2 shows the equipment for SB tests. The specimens, having 28-mm width, were cut from 16.6-mm nominal thickness line pipe, in transversal direction. The external surface of the specimen extracted from the pipe was preserved. During monotonic tests, the bending rate was regulated in order to induce strain rates in the range of the abovementioned SSR tensile tests. FEM modeling was carried out, using the software DEFORM™-2D (Columbus, OH, USA) for evaluating strain distribution along the specimen (Cabrini et al., 2008a,b).

The ripple loading slow bending (RLSB) tests were carried out by applying an initial ramp at 0.2 mm/s bending deflection rate. Afterwards, sinusoidal cycles were carried out at 10^{-2}-Hz frequency in order to induce cyclic reduction of load of about 10%, for 15 days.

Table 1: Chemical composition and mechanical properties of tested steels.

Steel (API 5L)	Chemical composition (%weight)					Mechanical properties (MPa)		Grain size
	C	Mn	Si	P	S	YS (0.2)	UTS	ASTM
x52	0.073	1.77	0.23	0.03	0.02	343	556	11
x65A	0.095	1.75	0.25	0.03	0.01	460	580	11
x65B	0.081	1.50	0.21	0.02	0.01	462	582	12.5

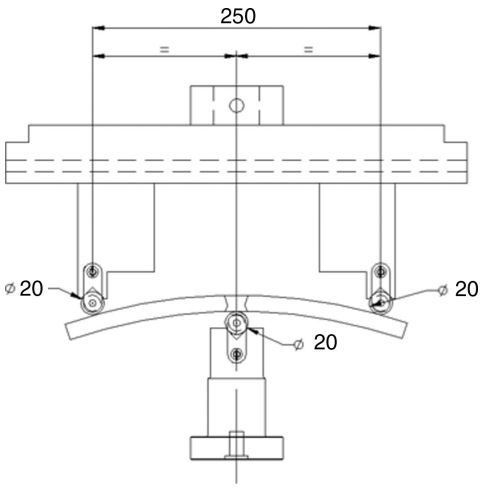

Figure 2: Equipment for SB tests.

3.2 Corrosion fatigue tests

Fatigue and corrosion-fatigue crack growth tests were performed on SENB3 specimens according to the requirements of the ASTM E647 standard. The experimental procedure was developed in a previous research (Cigada et al., 1985). Crack size (a_N) was evaluated through compliance (C_N) method by following equation, derived by ASTM E399-90 Standard:

$$\frac{a_N}{W} = 0.9997 - 3.95 \cdot U + 2.98 \cdot U^2 - 3.214 \cdot U^3 + 51.52 \cdot U^4 - 113.0 \cdot U^5 \quad (2)$$

$$U = \frac{1}{1 + \sqrt{4 \cdot E' \cdot B \cdot C_N \cdot \left(\frac{W}{S}\right)}}, \quad (3)$$

where

B = specimen thickness,
W = specimen width,
S = span length,
E' = Young's Modulus (E) for plane stress or $E/(1-\nu^2)$ for plane strain, and
ν = Poisson's ratio.

Crack growth rates (da/dN) were estimated by fitting crack length and cycle number (N) through an incremental second-order polynomial method on 25 successive points. The stress intensity factor range (ΔK) was evaluated according to ASTM E399 Standard by the following equation (ΔP_N is load range):

$$\Delta K = \left(\frac{\Delta P_N \cdot S}{B \cdot W^{\frac{2}{3}}}\right) \cdot f\left(\frac{a_N}{W}\right) \quad (4)$$

$$f\left(\frac{a_N}{W}\right) = \frac{3 \cdot \left(\frac{a_N}{W}\right)^{\frac{1}{2}} \cdot \left\{1.99 - \left(\frac{a_N}{W}\right) \cdot \left(1 - \frac{a_N}{W}\right) \cdot \left[2.15 - 3.93 \cdot \frac{a_N}{W} + 2.7 \cdot \left(\frac{a_N}{W}\right)^2\right]\right\}}{2 \cdot \left(1 + 2 \cdot \frac{a_N}{W}\right) \cdot \left(1 - \frac{a_N}{W}\right)^{\frac{3}{2}}} \quad (5)$$

A sinusoidal load was imposed with minimum to maximum load ratio R equal to 0.6, at 20-Hz and 0.2-Hz frequency for the tests in air and in solution, respectively.

Two types of test were performed. In constant-force-amplitude fatigue tests, load range is constant so that the stress intensity factor range increases during crack propagation. In K decreasing fatigue crack growth test, the load range decreases for producing a decreasing stress intensity factor range during crack propagation.

3.3 Electrochemical tests

Electrochemical tests were carried out in an ASTM G5-82 standard cell on specimens having1-cm^2 exposed area. The surface was grinded with 1200 grit silicon carbide emery paper, and then it was degreased with acetone in ultrasonic bath. Both fixed and rotating electrodes were used.

Cyclic potentiodynamic tests were carried out at 0.24 mV/s scan rate and a vertex potential of 1.24 V vs. NHE.

Cyclic voltammetries were performed. Ten cycles from −0.76 to +1.2 V vs. NHE or from −0.76 to +0.64 V vs. NHE were applied at 20 mV/s scan rate after 240 s of conditioning at −0.76 V vs. NHE, followed by 15 s of stabilization at free corrosion potential.

4 Results and discussion

4.1 Effect of dynamic loading

Despite the relevant number of laboratory tests, NN-SCC never occurred under constant loading during either axial tensile tests or U-bend tests. Thus, continuous deformation techniques were basically selected to assess susceptibility under variable loading. The presence of brittle areas on the fracture surfaces demonstrated NN-SCC occurrence during SSR test (Figure 3).

Consequently, the main point related to NN-SCC cracks occurrence remains the dynamic strain. Ripple loading tests and corrosion fatigue tests are representative of loading conditions that generate crack colonies

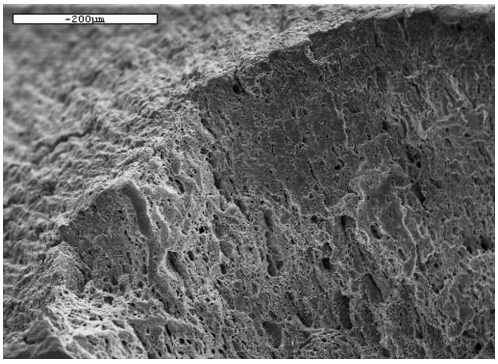

Figure 3: Brittle crack growth on fracture surface after SSR test in NS4 solution saturated with 5% of CO_2 at pH 7.

oriented along the axis of the pipe due to the fluctuation of internal gas pressure.

Monotonic slow strain rate tests – both uniaxial and bending – are representative of loading inducing transversal cracking, which is mainly caused by movements of ground in unstable areas that produce severe levels of loading up to plastic deformation field.

ISSR tests confirmed that continuous plastic deformation is necessary to promote cracks propagation. The crack embryos initiated during the plastic deformation phase did not propagate once the plastic deformation was interrupted (Figure 4). The same morphologies, i.e. small cracks initiated from shallow pit, were observed also after SB tests. Such cracks do not propagate even under ripple loading at small amplitude, up to 10% of maximum load.

However, at higher amplitudes – proper of fatigue phenomena – enhancement of crack propagation due to environmental effects was observed (Figure 5). The results of crack growth fatigue tests on SENB3 carried out

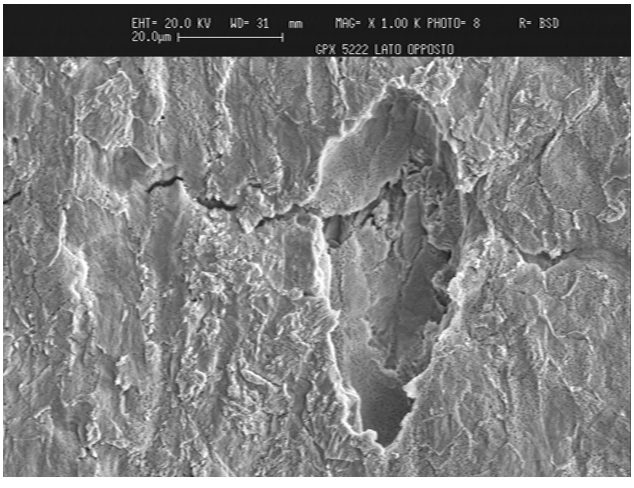

Figure 4: Crack embryo initiated from pit during ISSR tests on API 5L X52 in NS4 solution saturated with CO_2 at 0.05 bar and pH 7 at the free corrosion potential.

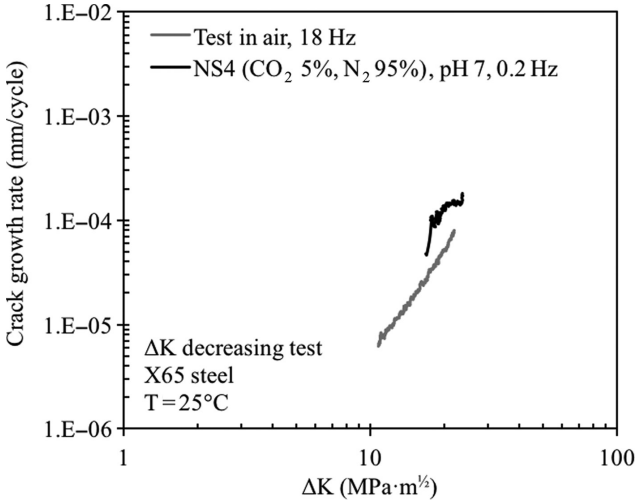

Figure 5: da/dN vs. ΔK fatigue test and C-F in the NN-SCC environment on SENB3 samples of X65 steel X65 ($R=0.6$; frequency in air 18 Hz, environment NN-SCC 0.2 Hz).

in NS4 solution saturated with N_2/CO_2 at 5% (pH 7) show an increase of crack growth rates. At 20 MPa $\sqrt{m}$ stress intensity factor range (ΔK), the fatigue crack growth rates in NS4 solution achieve values about 2.5 times higher than in air. According to superposing model proposed by Wei and Landes for stress corrosion fatigue, the difference can be considered as the contribution to propagation assisted by SCC. Thus, an estimation of crack growth rate in the environment promoting NN-SCC can be achieved under cyclic loading at low frequencies. According to the model, the crack growth can be assumed to be the sum of a contribution from pure fatigue, evaluated by means of the Paris' law $(da/dN)_F$ from air tests and a contribution due to crack growth from SCC $(da/dN)_C$.

$$\left(\frac{da}{dN}\right)_{C-F} = \left(\frac{da}{dN}\right)_F + \left(\frac{da}{dN}\right)_C \quad (6)$$

The crack growth rate due to NN-SCC can be estimated at 3×10^{-5} mm/s by considering that crack grows only during the increasing phase of the loading cycle, according to the relationship:

$$\left(\frac{da}{dt}\right)_{NN-SCC} = 2\cdot f\cdot\left(\frac{da}{dN}\right)_C \quad (7)$$

Our estimation refers to stable crack propagation and gives higher values compared to data reported by Parkins (National Energy Board, 1996). Parkins published that several laboratory data obtained on smooth specimens at maximum load of 108% of the TYS and an asymmetrical ratio R of 0.5 show that crack growth rates can vary from 10^{-9} mm/s to 10^{-6} mm/s. He suggested that SCC growth is characterized by periods of dormancy and rapid growth.

Our estimation is substantially related only to a stable subcritical crack grow of crack having large dimension, neglecting the dormancy period. It substantially confirms that the crack growth rate can be much higher once stable growth conditions are reached.

Ahmed et al. reported average crack growth rate from 1.4×10^{-9} mm/s to 7×10^{-7} mm/s, depending upon applied load range; they attributed the crack growth to corrosion fatigue for the more severe loading conditions in the short-term tests, while the growth was attributed to transgranular SCC under the less severe loading conditions of a high R ratio and low frequency (Ahmed et al., 1997). On the contrary, Chen and Sutherby (2007) reported that the crack growth behavior of pipeline steels in near-neutral pH environments is consistent with that of true corrosion fatigue, and the crack growth rate da/dN can be correlated with ΔK^2 Kmax/$f^{0.1}$.

The role of frequency was also investigated in literature. Although fatigue crack growth rate in air is insensitive to load frequency, the crack growth rate in near-neutral pH solution is very frequency-dependent. Crack growth rate was found to increase with decreasing loading frequency until 10^{-3} Hz, while it either remained constant for the underload-type variable amplitude cyclic loadings or decreased slightly for the constant amplitude loading when the loading frequency was lower than 10^{-3} Hz (Yu et al., 2015). A theoretical model – based on hydrogen effects on the crack tip during the cyclic load condition – was developed by Yu et al. to understand the crack growth behavior transition (Xing et al., 2015; Yu et al., 2015). The loading frequency must be low enough to create synchronized interactions at the crack tip between diffusible atomic hydrogen and cyclic loading, which appears very critical to crack growth rate. They assumed that the crack growth reaches a maximum rate when the hydrogen concentration at the crack tip reaches a certain value and the hydrogen equilibrium concentration in the plastic zone depends on the applied stresses. Therefore, the critical frequency separating the different growth behavior depends on the hydrogen diffusion into/out of the plastic zone, in response to the variation of stresses. The model suggests that this critical frequency depends on loading condition, temperature, mechanical properties of the steel, and hydrogen diffusivity at the crack tip, and it is estimated that the critical frequency is of the order of 10 – 3 Hz (Chen, 2016; Zhao et al., 2016a,b).

4.2 NN-SCC mechanism

Figure 6 shows the effect of the potential and temperature on EI from SSR tests in NS4 solution saturated with 0.05 bar CO_2 and N_2 at pH 7. At temperatures of 5°C and 25°C, SCC does not occur on anodically polarized specimens, but brittle areas were observed on fracture surface of both specimens at free corrosion potential and under cathodic polarization. The EI of these specimens increased as the potential decreased, as typical of a HE mechanism. At 50°C, SCC was only noticed on specimens under cathodic polarization. No SCC was found at 70°C, both at free corrosion potential and under cathodic polarization. SCC occurred only on the specimens under anodic polarization. Such temperature is typical of CB-SCC.

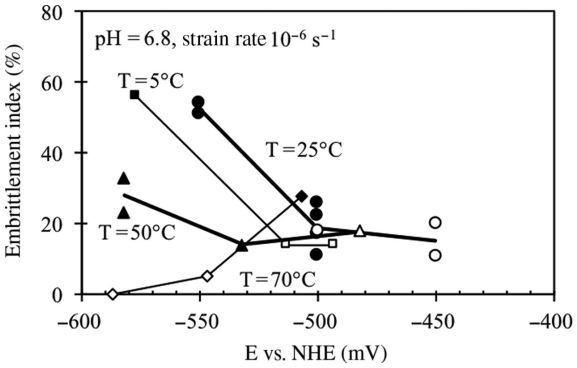

Figure 6: EI for X65 samples tested in NS4 solution at pH = 6.8 at different temperature and potentials after slow strain rate test (strain rate = 1.1×10^{-6} s^{-1}). Blank marks = NO SCC; full marks = SCCC.

Many authors ascribe to hydrogen a fundamental role in NN-SCC (Parkins et al., 1994; Liu & Mao, 1995; Cheng, 2013). Cheng demonstrated hydrogen entry into X70 steel at free corrosion potential. A correlation between NRA obtained by SSR tests and the concentration of hydrogen absorbed on the external surface of the metal was also proposed (Cheng, 2007a,b). Cheng and Niu (2007) reported that the electrolytes extracted from soils with previous SCC history were always associated with high hydrogen permeation currents and sub-surface hydrogen concentrations.

The results of SSR tests at different strain rates carried out both at free corrosion potential and under ±50-mV polarization (Figures 7 and 8) confirm the HE mechanism. Figures show the effect of the strain rate on the EI at pH 5.5 and 7. The specimens show an increase in the EI under cathodic polarization, as strain rate decreases. Such behavior is typical of HE mechanisms, and it is more evident at pH 5.5 rather than at pH 7. The effect of the strain rate cannot be observed at free corrosion potential – independently upon pH – whereas the SCC phenomena do not occur at all under anodic polarization.

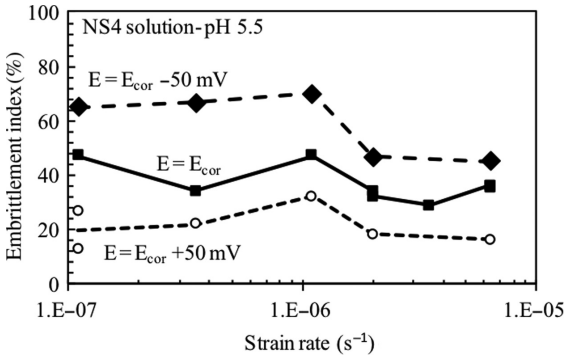

Figure 7: Effect of the strain rate on reduction of area ratio in NS4 solution saturated with CO_2 for samples potentiostatically controlled in anodic (circle), free corrosion (square), and cathodic potential (rhombus). Blank marks = NO SCC; full marks = SCC; at pH 5.5.

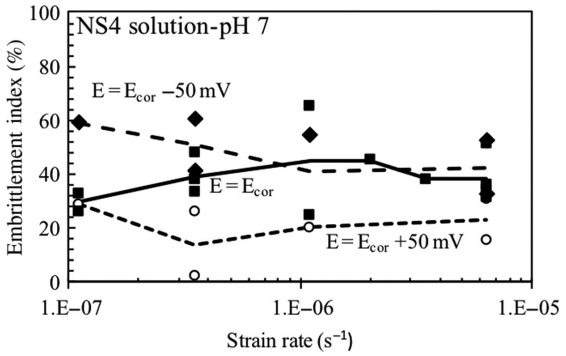

Figure 8: Effect of the strain rate on reduction of area ratio in NS4 solution saturated with CO_2 for samples potentiostatically controlled in anodic (circle), free corrosion (square), and cathodic potential (rhombus). Blank marks = NO SCC; full marks = SCC; at pH 7.

4.3 Role of localized corrosion

The NN-SCC cracks observed after laboratory tests always initiated from localized attacks on the steel surface, in zones where severe general corrosion attack also occurred (Figure 4). Several authors highlight that localized attacks played a fundamental role for NN-SCC crack initiation.

According to Elboujdaini et al. (2000) and Eslami et al. (2010), the NN-SCC cracks can initiate from micropits under cyclic load conditions due to strain concentration. In the absence of pits, cracks initiated from machining defects or emerging bands of deformation (Eslami et al., 2011).

Always according to Eslami et al., the presence of pearlitic phases inside the pits increases the dissolution rate of the surrounding areas due to galvanic effect and makes the base sharper. In this manner, the stress concentration effect increases, favoring the initiation of cracks (Eslami et al., 2010).

Beavers et al. (2000) outline the role of residual internal stress. Residual stresses exist on both macroscopic scale, due to the pipe production process, forming and lay, and microscopic scale, due to ferrite-pearlite banding or segregations. Van Boven et al. (2007) stated that macroscopic residual tensile stresses are responsible for pit and crack initiation. The formation of micro-pitting was found to occur preferentially in areas where the tensile residual stresses were the highest, while SCC initiation occurred mainly in areas where the surface residual stress was in an intermediate range. The difference between residual stress levels occurring at SCC locations vs. pitting locations resulted from both the change of residual stress during cyclic stress application during SCC testing and the residual stress gradient in the depth direction.

Figure 9 shows the mechanism for the initiation of the NN-SCC from localized attacks (Cabrini & Sinigaglia, 1996a,b). The presence of localized attacks can favor hydrogen development inside the pit, due to the increase of acidity and the absence of corrosion scales, with respect to the external areas covered by corrosion products.

The presence of undissolved cementite, which has a low overvoltage, further promotes the hydrogen evolution. Crolet et al. suggest the possibility of a microstructurally formed galvanic coupling between steel (ferrite phase) and cementite (Fe_3C). In fact, cementite is nobler than ferrite and remains undissolved on the steel surface. Then, the galvanic coupling led to local acidification and to the dissolution of iron carbonate (Crolet et al., 1998).

In the presence of plastic strain, hydrogen causes brittle rupture at the maximum tensioned zone placed at pit tip. Crack embryo can form under such conditions. The probability of crack embryo propagation depends on the balance between the brittle tip hydrogen assisted

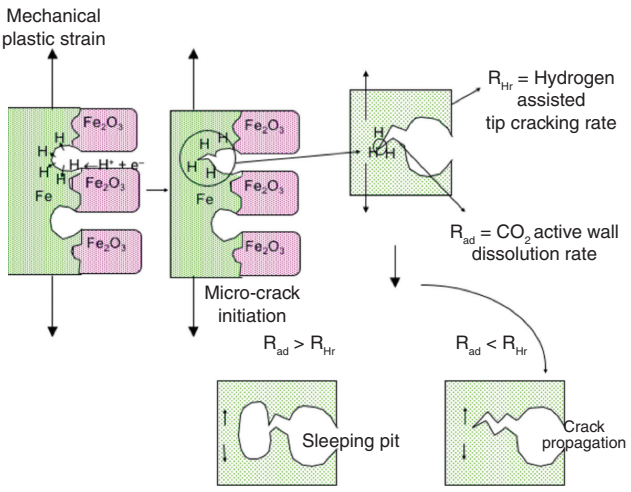

Figure 9: Schematic representation of NN-SCC initiation from pit.

cracking rate (R_{Hr}) and the CO_2 assisted general corrosion of the crack walls (R_{ad}). If R_{Hr} is lower than R_{ad}, the crack becomes enlarged and transforms into a pit. Parkins called these "sleeping pits" because they are unable to promote further cracks (National Energy Board, 1996). If R_{Hr} is higher than R_{ad}, the crack can reach the critical size that allows it to propagate.

A recent work of Zhao et al. (2017a,b) presenting the statistical analysis of the cracks on an exercised pipeline pointed out that the first stage of crack initiation is fast owing to the high internal stress on the outer pipe surface and usually leads to dormant cracks with a depth of about 1.0 mm. Only less than 5% of cracks are able to grow out of the dormant state (Zhao et al., 2017a,b).

Figure 10 shows examples of a sleeping pit (Figure 10A) and microcrack that can grow (Figure 10B) on SSR specimens that were electrochemically pre-corroded before the test.

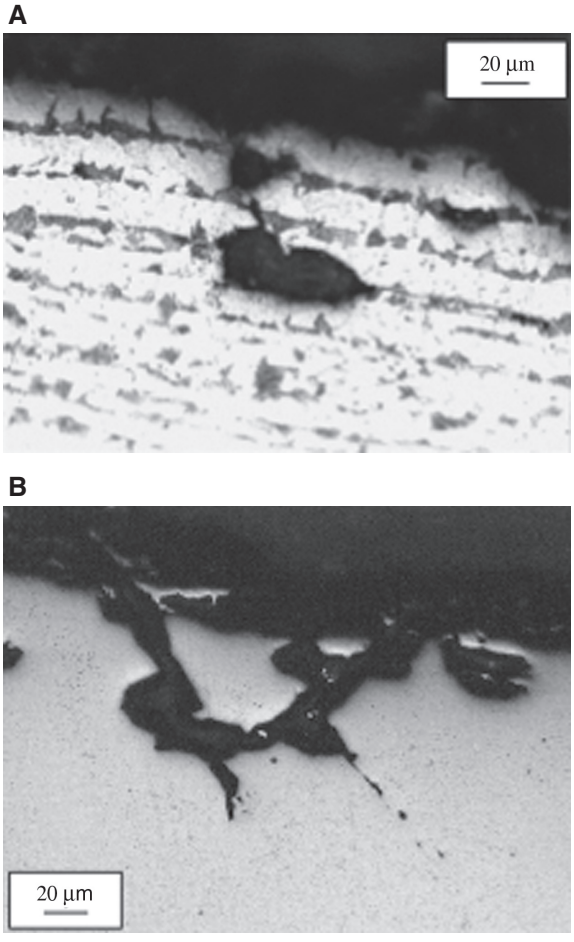

Figure 10: Metallographic section of API 5L X52 specimens electrochemically pre-corroded at the end of the SSR tests in NS4 + 12.2 g/l of $NaHCO_3^-$ solution saturated with CO_2 at pH 7; (A) sleeping pit from a crack embryo; (B) crack growing.

The importance of the "dormant" stage in NN-SCC cracks is highlighted by Chen et al. (2007), who confirmed that the majority of NN-SCC cracks that nucleate during operation stop propagating before reaching depths above 1 mm. This depth generally does not compromise pipe integrity. In the case of the large-diameter pipes of the Canadian lines subject to NN-SCC, it corresponds to approximately 10% of the wall thickness. These pipelines are generally used at pressures that limit the circumferential force to below 72% of the minimum guaranteed yield strength; the faults are therefore widely tolerable. Only an extremely small percentage of NN-SCC cracks reach the critical depths that can cause pipe breakage.

In the dormant phase, the cracks take on a rounded shape because of the high general corrosion of the walls; in addition, they no longer advance until the stress conditions at their apexes change.

Parkins highlights that checking the lines with hydraulic tests can influence this phase of crack life, causing re-activation of dormant cracks or, on the contrary, plasticising the tip of the embryo cracks and transforming them into dormant cracks (National Energy Board, 1996).

Experimental data collected in slow strain rate condition (Figure 11) emphasized the role of pH in NN-SCC occurrence. The tests were carried out in NS4 solution or in Na_2SO_4 0.1 M solution saturated with Co_2 at different pH. A full mark indicates SCC occurrence, while a blank mark indicates the absence of SCC. The highest value of the EI was measured on the samples tested at pH values around 7, while no SCC phenomena were noticed at all at pH values exceeding 7.5. The cracks always initiated from small pits.

At the free corrosion potential, the hydrogen source for the embrittlement mechanism is produced only by the

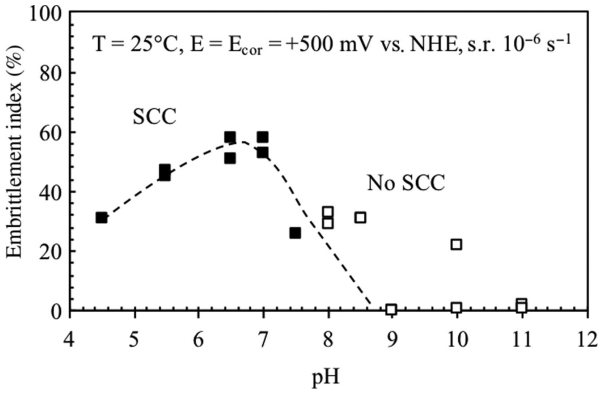

Figure 11: Embrittlement index for X65a samples tested in NS4 solution at different pH and CO_2 concentration after slow strain rate test ($\varepsilon' = 1.1 \times 10^{-6}$ s^{-1}). Blank marks = NO SCC; full marks = SCC.

cathodic reactions associated with the anodic dissolution of the steel (R_{ad}).

In neutral solution and in the absence of oxygen, the cathodic reaction associated with steel corrosion is the reduction of hydrogenions produced by the water dissociation (8) and (9) or water reduction (10):

$$2H_2O \rightleftarrows H_3O^+ + OH^- \quad (8)$$

$$H_3O^+ + e^- \rightarrow \frac{1}{2}H_2 \quad (9)$$

$$H_2O + e^- \rightarrow \frac{1}{2}H_2 + OH^- \quad (10)$$

The presence of H_2CO_3 can increase the corrosion rate in two different ways. Dissociation of H_2CO_3 (11):

$$H_2CO_3 + H_2O \rightleftarrows H_3O^+ + HCO_3^- \quad (11)$$

serves as an additional source of H_3O^+ ions (Bonis & Crolet, 1989), which are subsequently reduced according to Equation (9). In addition, there is a possibility of the direct reduction of H_2CO_3 (12) (De Waard & Milliams, 1975; Eriksrud & Søntvedt, 1984; Gray et al., 1989; Nordsveen et al., 2003):

$$H_2CO_3 + 2e^- \rightarrow H_2 + 2HCO_3^- \quad (12)$$

and, above pH 5, even a reduction of the bicarbonate ion, HCO_3^- (13) (Gray et al., 1990):

$$2HCO_3^- + 2e^- \rightarrow H_2 + 2CO_3^{2-} \quad (13)$$

It has been suggested that the direct reduction of the bicarbonate ion (Ogundele & White, 1987; Gray et al., 1990) and water (Nešić et al. 1996a,b) can become important at low CO_2 partial pressures and high pH, but at the same time, when the pH increases from 6 to 7, the precipitation of the corrosion product can be fast, reducing the corrosion rate by means of protective corrosion product films (Dugstad, 2015). The reduction in the corrosion rate of steel reduces hydrogen evolution at the same time.

Inside the localized attacks, the precipitation of corrosion products cannot take place owing to absence of bicarbonate and carbonate ions, so the hydrogen absorption can take place on the bare metal surface. As previously illustrated, the cracks can grow if the hydrogen assisted tip rupture rate, R_{Hr}, is higher than the metal anodic dissolution rate, R_{ad}. Decreasing the strain rate, both these two rates increased, and the two effects compensate each other, preventing a net increase of the NN-SCC phenomena as the strain rate in the SSR tests shown in Figure 9 decreases.

The proposed mechanism confirms the mechanism hypothesized by Parkins, which considers the synergic action of hydrogen entrance and the active dissolution of the steel inside the NN-SCC crack. According to Parkins, NN-SCC occurs through the contemporary dissolution of the walls and tip of the crack, in the absence of passive films, and is accompanied by the entrance of hydrogen into the steel (National Energy Board, 1996). Similar considerations were analyzed more recently by Liu et al. (2012).

Cheng (2007a,b) developed a thermodynamic model to illustrate the interactions of stress, hydrogen, and anodic dissolution at the crack tip. He affirmed that the growth rate of NN-SCC depends on the synergistic effect of hydrogen and stress on the anodic dissolution rate of steel at crack tip and the effect of the concentration difference of hydrogen atoms between the stressed and the unstressed steel on the anodic dissolution reaction (Cheng, 2007a,b).

Gu et al. (1999) and Mao et al. (2001) suggested that SCC was controlled by a hydrogen-facilitated anodic dissolution mechanism. On the other hand, Lu et al. reported that the crack propagation of pipeline steel in near-neutral pH groundwater is mainly dominated by the dissolved hydrogen concentration and is less influenced by anodic dissolution; the dependence of the resistance of pipeline to the EAC in near-neutral pH groundwater can be interpreted using an improved corrosion-facilitated plasticity model (Lu et al., 2009, 2010).

4.4 Pitting formation

In this work, the conditions for the insurgence of localized attacks in CO_2/HCO_3^- at neutral pH were investigated by means of cyclic potentiodynamic and cyclic voltammetry tests.

Figure 12 shows the effect of bicarbonate ions concentration on the cyclic potentiodynamic curves for a X65 steel. All the steels examined in this experimental work showed similar electrochemical behavior. In NS4 solution at pH 7, fully active behavior was observed.

An initial increase of the anodic dissolution current was noticed by increasing the bicarbonate ion concentration at 4.83 g/L, balanced by an increase in the CO_2 partial pressure to maintain a constant pH. The current density decreases as the potential rises up to 0.6 V vs. NHE. As the potential scan was inverted, the anodic current continued to decrease until a further increase occurred at about −0.3 V vs. NHE, and the direct and reverse curves became then overlapped.

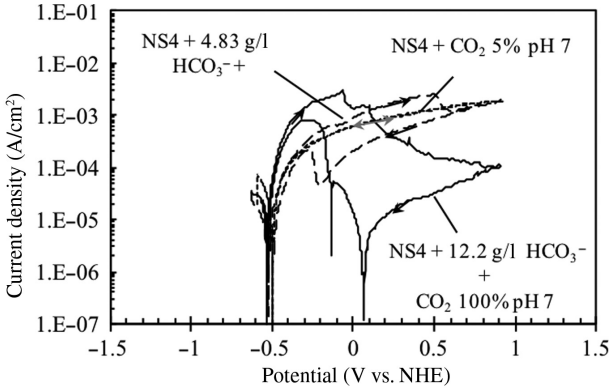

Figure 12: Potentiodynamic tests of API 5L X65 in NS4 solution with different concentrations of HCO_3^- ions.

A further increase of the CO_2 pressure and bicarbonate concentration causes an initial increase of the anodic current, followed by a decrease when the applied potential approaches 0 V vs. NHE. The anodic current continues to decrease also in the reverse potential scan. In this solution, the specimens showed three equilibrium potentials, one at about +0.1 V vs. NHE, the other at about −0.2 V vs. NHE, and the last one at free corrosion potential (−0.52 V vs. NHE).

Figure 13 shows the effect of the rotational speed of the electrode on the potentiodynamic curves in the solution with the highest bicarbonate concentration. When the rotating electrode rate was increased from 0 to 100 rpm, the anodic current slightly increases and the potential at which it becomes decreased is nobler than the curve in static conditions. The equilibrium potentials in the reverse scan shift toward more cathodic values. A further increase of rotational speed of the electrode causes an increase of the anodic current. The potential at which the current density decreases remains constant, and the free corrosion potential shifts toward 0 V vs. NHE.

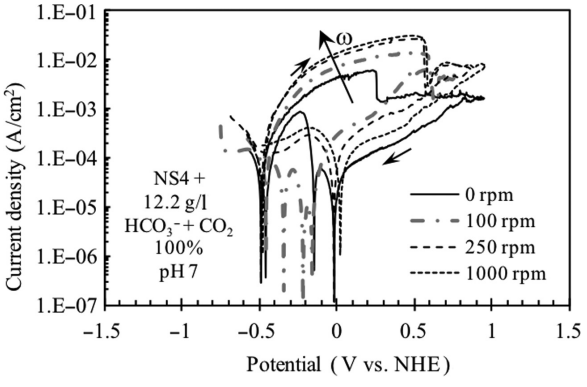

Figure 13: Potentiodynamic tests of API 5L X65 in NS4 solution + 12.2 g/l of $NaHCO_3^-$ at different electrode rotating rate (E vs. NHE).

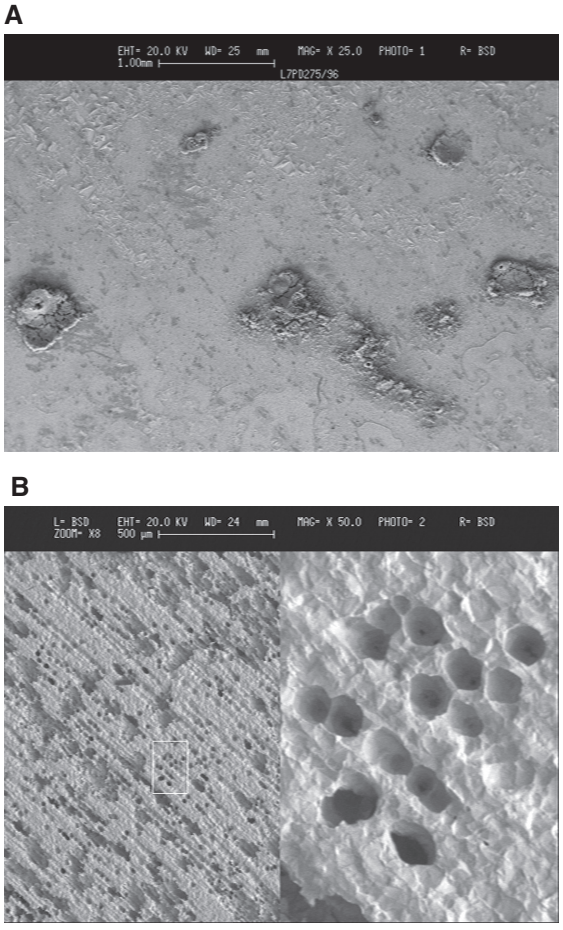

Figure 14: SEM images of the specimens of API X65 steel after potentiodynamic tests in NS4 + 12.2 g/L of $NaHCO_3$ solution (A) at 0 rpm; (B) at 100 rpm.

The anodic current was always very high in these conditions, so the formation of a stable passive film cannot be stated. However, a certain modification in the corrosion morphology can be observed. The specimens tested in high bicarbonate solution and at low rotational speeds of the electrode showed localized attacks (Figure 14A), while pitting was not noticed at rotational speeds exceeding 250 rpm. The morphology observed at the end of the tests at higher rotational speeds was characterized by the presence of deep corrosion pits where hot rolling bands are visible and pits with a rounded form (Figure 14B).

Cyclic voltammetry is quite a different non-stationary technique compared to traditional potentiodynamic technique. High scan rate of 20 mV/s permits to highlight the reaction transients. The growth and stabilization of the species that form on the electrode surface, as well as the reversibility of the involved reactions, can be assessed by the execution of several consecutive potential scans.

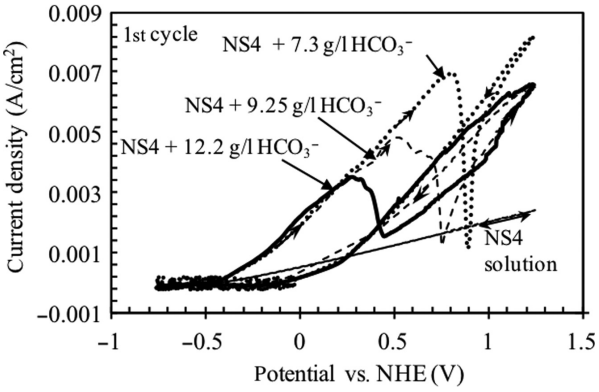

Figure 15: Current vs. potential curves in the cyclic voltammetry tests at 20 mV/s and 0 rpm in NS4 with different concentration of $NaHCO_3$ at pH 7.

In NS4 solution saturated with CO_2, active dissolution occurs without the formation of intermediate film. Therefore, the cyclic voltammetry curve does not show any peak as reported by Wieckowski et al. (1983) (Figure 15). Similar behavior was observed on API X70 steel by Niu and Cheng (2007).

An anodic peak can be noticed as the bicarbonate concentration in the solution increases (Figure 15). The amplitude of the peak decreases with the number of cycles (Figure 16). The peak is not present in the cathodic scans due to the irreversibility of the reaction. The presence of such peak in the cyclic voltammetry curves is strongly influenced by diffusion. The peak becomes less defined and gradually disappears as the rotational speed of the electrode rate increased. Active steel corrosion is then observed as for solutions with low bicarbonate ions concentration (Figure 17).

The presence of the peaks in the voltammetry curves is associated with the presence of localized attack on the specimen surface.

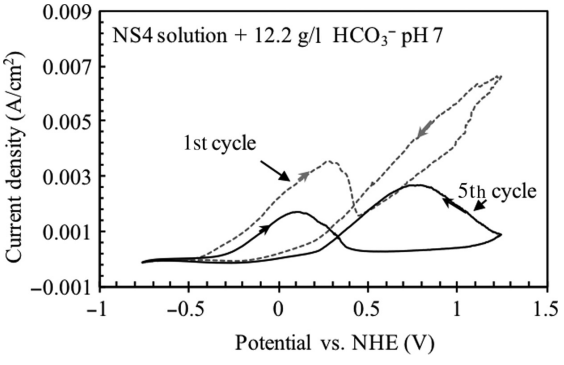

Figure 16: Current vs. potential curves in the cyclic voltammetry tests in NS4 + 12.2 g/l of $NaHCO_3$ at pH 7 (20 mV/s and 0 rpm).

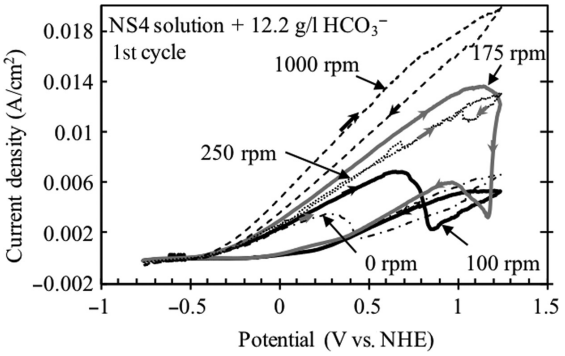

Figure 17: Current vs. potential curve in the cyclic voltammetry tests in NS4 + 12.2 g/l of $NaHCO_3$ at pH 7 (20 mV/s) and different rotating electrode rates.

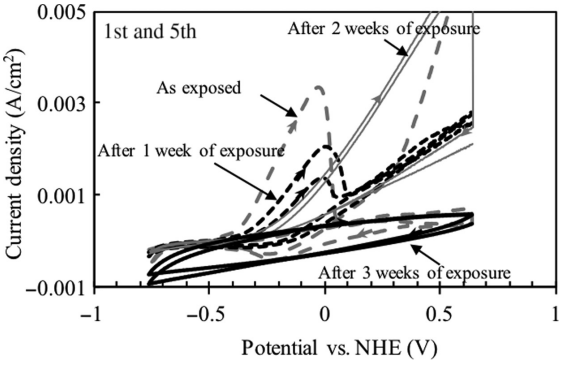

Figure 18: Current vs. potential curve in the cyclic voltammetry tests in NS4 + 12.2 g/l of $NaHCO_3$ at pH 7 (20 mV/s) on specimens just immersed or immersed in the solution from 1 to 3 weeks.

Figure 18 reports the cyclic voltammetry curves obtained in NS4 solution with 12.4 g/L HCO_3^-, at pH 6.8 as a function of exposure time. The peak current decreased with exposure time, but very low anodic current was observed, meaning that a stable film formed.

The electrochemical behavior could be interpreted on the basis of the different reaction that can take place on the specimen's surface.

The mechanism suggested by Bockris et al. (1961) for the reactions of iron dissolution in neutral or acid solution hypothesizes the formation of an intermediate stage of hydroxide caused by reaction (14–16) (Dugstad, 2015):

$$Fe + H_2O \Leftrightarrow FeOH + H^+ + e^- \quad (14)$$

$$FeOH \xrightarrow{rds} FeOH^+ + e^- \quad (15)$$

$$FeOH^+ + H^+ \Leftrightarrow Fe^{2+} + H_2O \quad (16)$$

The presence of CO_2 in the solution avoids hydroxide intermediate formation. Davies and Burstein (1980) proposed that HCO_3^- ions act directly in the electrochemical

dissolution through the formation of a soluble complex $Fe(HCO_3)_2$ as illustrated in the following reaction (17–19):

$$Fe + HCO_3^- \rightarrow FeCO_3 + H^+ + 2e^- \quad (17)$$

$$Fe + 2HCO_3^- \rightarrow Fe(HCO_3)_2 + 2e^- \quad (18)$$

$$FeCO_3 + HCO_3^- \rightarrow Fe(CO_3)_2^{2-} + H^+ \quad (19)$$

More recently, Nešić et al. (1996a,b) proposed the formation of a complex Fe-CO_2, called Fe_L, in the mechanism for iron dissolution in CO_2 containing solution at pH above 5:

$$Fe + CO_2 \Leftrightarrow Fe_L \quad (20)$$

$$Fe_L + H_2O \Leftrightarrow Fe_LOH_{ad} + H^+ + e^- \quad (21)$$

$$Fe_LOH_{ad} \overset{rds}{\rightarrow} Fe_LOH^+_{ad} + e^- \quad (22)$$

$$Fe_LOH^+_{ad} + H_2O \Leftrightarrow Fe_L(OH)_{2ad} + H^+ \quad (23)$$

$$Fe_L(OH)_{2ad} \Leftrightarrow Fe_L(OH)_{2sol} \quad (24)$$

$$Fe_L(OH)_{2sol} + 2H^+ \Leftrightarrow Fe^{2+} + CO_2 + 2H_2O \quad (25)$$

They assumed that the complex formed as an adsorbed species on the surface of the electrode that catalyzes the dissolution of iron.

The mechanism described in reactions (17–19) or (10–25) is compatible with the active dissolution of steel in an NS4 solution saturated with CO_2 at pH 7 or lower.

These conditions do not favor the formation of a protective film of iron carbonate on carbon steel. In spite of this, if the active dissolution reaction of iron takes place in a reduced volume of electrolyte – as water condensation occurs inside the detached coating – it can be hypothesized that the Fe^{2+} coming from active dissolution of the steel and CO_3^{2-} ions, due to the dissociation of the bicarbonate ions, which lead to the precipitation of iron carbonate, reach conditions of supersaturation. In the electrochemical tests in solution, this condition is reached when the concentration of CO_2 and bicarbonate ions in solution was increased.

The precipitation of iron carbonate occurs as the anodic current decreases in the potentiodynamic curves. Such reaction does not appear as a peak on the voltammogram because it does not involve the exchange of electrons.

The subsequent oxidation from iron carbonate to $Fe^{(III)}$ oxide/hydroxide can be observed as a peak on the voltammetry curve. The peak potential is not constant, but it becomes nobler by increasing the bicarbonate ions concentration.

The presence of an equilibrium of the species $FeCO_3$/$Fe^{(III)}$ oxide/hydroxide, associated to the presence of localized attack, is confirmed by the equilibrium potential at 0 V observed during the reverse scan of potential in potentiodynamic tests. The equilibrium potential of reaction (26),

$$\gamma Fe_2O_3 + 2CO_3^{2-} + 6H^+ + 2e^- \rightleftarrows 2FeCO_3 + 3H_2O \quad (26)$$

$$E° = 1.48 - 0.177\,pH + 0.059\log([CO_3^{2-}]), \quad (27)$$

is 0 V vs. NHE for a carbonate concentration of 8×10^{-5} mol/L. This value is independent upon the rotational speed of the electrode.

As the carbonate film does not fully cover the metal surface, when the oxide forms on the metal surface, there are areas covered by the oxide and areas without any scale. In these conditions, localized attack was initiated, as shown in Figure 19.

The equilibrium potentials observed in the potentiodynamic tests at potential between 0 and –0.52 V vs. NHE could be related to the reduction of the oxidized species inside the localized attacks owing to the decreasing of the pH.

The role of the oxides in the localized attacks in NN-SCC is highlighted also by numerous authors. According to Parkins (National Energy Board, 1996), the composition of the solution in zones under the coatings can be subject to variations due to the higher or lower supply of CO_2 from the ground, connected, for example, to seasonal variations in the activity of the vegetation. Abedi et al. (2007) also reported intergranular cracks initiated

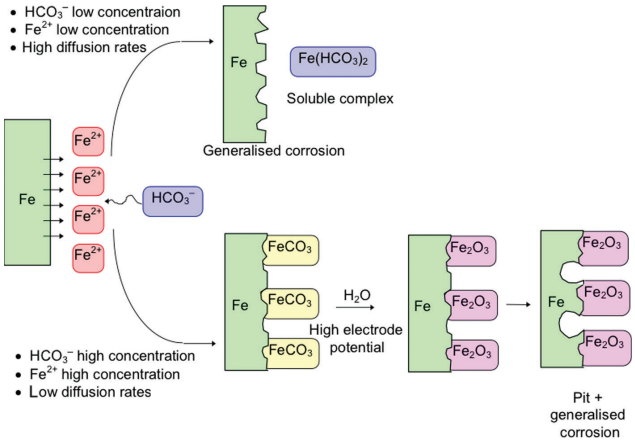

Figure 19: Schematic representation of pitting initiation during cyclic voltammetry tests.

by CB-SCC, which propagate in a transgranular manner with strong general corrosion, typical of NN-SCC. Parkins and Zhou report that the corrosion products in carbonate-bicarbonate environments have a bilayer structure, in conformity with the suggestions of Riley and Sykes (1990), with $FeCO_3$, complex ferrous-ferric oxides (γ-Fe_2O_3/Fe_3O_4 containing Na^+), and ferrous or ferric hydroxycarbonates, $Fe_x(OH)_y(CO_3)_z$, the latter increasing with increasing potential and temperature (Parkins & Zhou, 1997). Han et al. observed that the structure of the passive layer formed during spontaneous passivation at the open circuit potential in the presence of CO_2 and iron carbonate contains magnetite (Han et al., 2011). These products are compatible with the species formed during the voltammetry cycles, which promote the formation of localized attacks.

According to Elboujdaini et al. (2000), the formation of localized attacks is associated with the presence of non-metallic inclusions on the surface. Eslami et al. (2011) confirm that the initiation of micropits on the surface of steel occurs during the early immersion in the NS4 solution saturated with CO_2 at 0.05 bar and pH 7, in correspondence with microstructural non-uniformities on the steel surface. By interrupting the CO_2bubbling, the pH increases to values equal to approximately 10, and localized attacks were not observed (Eslami et al., 2011).

As several authors confirmed the fundamental role of localized corrosion, an electrochemical pre-corrosion procedure was than developed to obtain specimens with localized attacks to be used for testing. The surface of the specimens was grounded with emery paper up to 1200 grit, and then it was cleaned in acetone. Afterwards, the surface of specimens was coated to reduce the exposed surface. The pre-corrosion was achieved through a series of voltammetry cycles from –1 to +1 V vs. SCE at 20 mV/s of scan rate, for producing localized attacks. The cycles begin after 240 s of condition time at –1 V, followed by 15 s of stabilization time at free corrosion potential in the NS4 solution added with 12.4 g/L, saturated pure CO_2 at 1 atm.

These specimens showed a little increase of the EI respect to the specimens with machined surface. For example, the EI rises from 24% to 30% for the X52 steel and from 14% to 30% for the X65 steel. NN-SCC was always initiated from pre-formed pits (Figure 20).

Similar results were observed in a full scale test on electrochemically pre-corroded X100 pipelines after 1 year of exposure in NN-SCC environments under cyclic loading (Spinelli & Marchersani, 2004; Marchesani et al., 2005; Demofonti et al., 2008a,b).

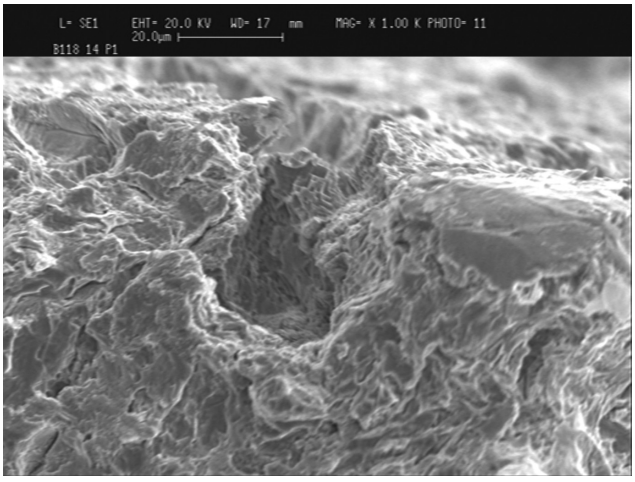

Figure 20: SSR specimens after SSR tests in NS4 + 12.2 g/l di $NaHCO_3$ solution saturated with 1 bar of CO_2 at pH 7 on electrochemically pre-corroded specimens of X52 steel.

5 Conclusions

In the present work, the results obtained by authors concerning NN-SCC of buried pipelines are reported. NN-SCC was not observed in constant load tests and constant deformation tests but only in slow strain rate tests. Microcracks initiated from localized attacks were observed during SB tests, ISSR, and SB ripple loading tests. Corrosion fatigue tests evidenced the possibility of an increase in the crack propagation in NS4 solution for ΔK higher than 20 MPa$\sqrt{m}$. The crack growth measured in these tests was higher than the field data for NN-SCC but comparable with laboratory tests.

Electrochemical tests (potentiodynamic and cyclic voltammetry) evidenced the role of bicarbonate ions and diffusion on localized attack initiation.

A pre-corrosion procedure was developed to reproduce localized attacks on the specimen surface having morphology similar to that observed on cracked pipelines, acting as a preferential site for crack initiation.

A mechanism for localized attack formation and NN-SCC initiation and propagation was proposed. NN-SCC cracks are nucleated inside the pit by HE under local plastic deformation conditions. Hydrogen was generated by the cathodic reaction complementary to the active dissolution of the steel. Carbonic acid and bicarbonate ions play an active role in this mechanism, enhancing hydrogen production and avoiding iron carbonate precipitation on the crack tip.

Acknowledgments: Our special thanks go to all those people who, for different reasons, collaborated in the research

carried out for this article. Because the list would be too long, their names can be found in the references section of this paper. Above all, our heartfelt thanks go to Pietro Pedeferri, whose teaching continues to live in those who had the fortune to be his students.

References

Abedi S, Abdolmaleki A, Adibi N. Failure analysis of SCC and SRB induced cracking of a transmission oil products pipeline. Eng Failure Anal 2007; 14: 250–261.

Ahmed T, Lambert S, Sutherby R, Plumtree A. Cyclic crack growth rates of X-60 pipeline steel in a neutral dilute solution. Corrosion 1997; 53: 581–590.

Baker Jr M, Fessler R. Pipeline Corrosion; final report. U.S. Department of Transportation Pipeline and Hazardous Materials Safety Administration Office of Pipeline Safety, Integrity Managment Program Under Delivery Order DTRS56-02-D-70036, 2008.

BeaversJ, Johnson J, Sutherby R. Materials factors influencing the initiation of near-neutral pH SCC on underground pipelines. In Proceedings of 3th International Pipeline Conference, 2, pp. 979–988, 2000, Calgary, Canada.

Bockris J, Drazic D, Despic A. The electrode kinetics of the deposition and dissolution of iron. Electrochim Acta 1961; 4: 325–361.

Bolzoni FM, Cabrini M, Pedeferri P, Sinigaglia E. Caratterizzazione elettrochimica di acciai per tubazioni interrate in presenza di CO_2/HCO_3^-. Atti del 4° Convegno "Giornate nazionali sulla corrosione e protezione dei materiali metalliciGenova, AIM, 1999: 257–266.

Bolzoni FM, Cabrini M, Pedeferri P, Hoxha G. Stress corrosion cracking of a buried flow line. In Proceedings of the International Conference "Corrosion in refinery petrochemical and power generation plants", Venezia; 2000: 75–82.

Bonis M, Crolet J. Basics of the prediction of the risks of CO_2 corrosion in oil and gas wells. In Proceedings of CORROSION/89 (CD paper no. 466). Houston, TX: NACE, 1989.

Cabrini M, Sinigaglia E. Effetto della temperatura e del potenziale sulla corrosione sotto sforzo di acciai microlegati in soluzione di HCO_3^- e CO_2. Atti del 3° Convegno Nazionale sulla Corrosione e Protezione dei Materiali. Milano: AIM, 1996a: 29–38.

Cabrini M, Sinigaglia E. Studio del meccanismo di corrosione sotto sforzo degli acciai basso legati in soluzione di CO_2/HCO_3^-. Atti del 3° Convegno Nazionale AIMAT '96, Omaggio scientifico a Riccardo Sersale, Napoli 1996b; 1: 424–433.

Cabrini M, Pistone V, Sinigaglia E, Tarenzi M. Unique Hsc scenario leads to gas line failure. Oil Gas J 2000; 6: 61–65.

Cabrini M, D'Urso G, Pastore T. Evaluation of the resistance to hydrogen embrittlement by slow bending test. In Shipilov S, Jones R, Olive J, Rebak R, Environment-induced cracking of materials - prediction, industrial developments and evaluation. 2008a; 2: 493–502.

Cabrini M, Lorenzi S, Marcassoli P, Pastore T. NN-SCC di un acciaio per tubazioni interrate. In: Atti del 9° Convegno Nazionale AIMAT. Piano di Sorrento, 2008b (CD).

Cabrini M, Lorenzi S, Marcassoli P, Pastore T. Studio della NN-SCC di acciai per tubazioni interrate tramite prove di flessione in tre punti. Metall Ital 2010; 3: 5–11.

Cabrini M, Lorenzi S, Marcassoli P, Pastore T. Hydrogen embrittlement behavior of HSLA line pipe steel under cathodic protection. Corros Rev 2011; 29: 261–270.

Cabrini M, Lorenzi S, Pellegrini S, Pastore T. Environmentally assisted cracking and hydrogen diffusion in traditional and high-strength pipeline steels. Corros Rev 2015; 33: 529–545.

Chen W. An overview of near-neutral pH stress corrosion cracking in pipelines and mitigation strategies for its initiation and growth. Corrosion 2016; 72: 962–977.

Chen W, Sutherby R. Crack, growth behavior of pipeline steel in near-neutral pH soil environments. Metall Mater Trans A 2007; 38: 1260–1268.

Chen W, Van Boven G, Rogge R. The role of residual stress in neutral pH stress corrosion cracking of pipeline steels – Part II: crack dormancy. Acta Mater 2007; 55: 43–53.

Cheng Y. Analysis of electrochemical hydrogen permeation through X-65 pipeline steel and its implications on pipeline stress corrosion cracking. Int J Hydrogen Energy 2007a; 32: 1269–1276.

Cheng Y. Fundamentals of hydrogen evolution reaction and its implications on near-neutral pH stress corrosion cracking of pipelines. Electrochim Acta 2007b; 52: 2661–2667.

Cheng Y. Stress corrosion cracking of pipelines - Wiley series in corrosion. New York, NY: John Wiley & Sons, 2013.

Cheng Y, Niu L. Mechanism for hydrogen evolution reaction on pipeline steel in near-neutral pH solution. Electrochem Commun 2007; 9: 558–562.

Cigada A, Mazza B, Pastore T, Pedeferri P. Fatigue crack growth of HSLA steel in seawater. Metals Materials Technology Series, ASM 8520-012, 1985: 1–7.

Crolet J, Thevenot N, Nešić S. Role of conductive corrosion products in the protectiveness of corrosion layers. Corrosion 1998; 54: 195–203.

Davies D, Burstein G. The effects of bicarbonate on the corrosion and passivation of iron. Corrosion 1980; 36: 416–422.

De Waard C, Milliams D. Carbonic acid corrosion of steel. Corrosion 1975; 31: 177–181.

Delanty B, O'Beirne J. Major field-study compares pipeline SCC with coatings. Oil Gas J 1992; 90: 39–44.

Demofonti G, Cabrini M, Marchesani F, Spinelli CM. Eni TAP project mechanical damage & environmental assisted cracking full scale methodology overview. Coppola T, editor. In Proceedings of ISOPE 2008 Vancouver (Canada): 2008a (CD).

Demofonti G, Cabrini M, Marchesani F, Spinelli CM. Eni tap project mechanical damage and environmental assisted cracking -full scale methodology overview. New developments on metallurgy and applications of high strength steels. Buenos Aires: John Wiley & Sons, 2008b: 1: 611–624

Dugstad A. Fundamental aspects of CO_2 metal loss corrosion, Part I: mechanism. In Proceedings of CORROSION/2015 (CD paper 5226). Houston (TX): NACE, 2015.

Elboujdaini E, Wang Y, Revie R, ParkinsR, Shehata M. Stress corrosion crack initiation processes: pitting and microcrack coalescence. In Proceedings of CORROSION/2000 (CD. paper 00379). Houston (TX): NACE, 2000.

Eriksrud E, Søntvedt T. Effect of flow on CO_2 corrosion rates in real and synthetic formation waters. Hausler RH, Goddard HP, editors. In Proceedings of Advances in CO_2 Corrosion, 83 Symp. on CO_2 Corrosion in the Oil and Gas Industry.1. Houston, TX: NACE, 1984: 20.

Eslami A, Fang B, Kania R, Worthingham B, Been J, Eadie R, Chen W. Stress corrosion cracking initiation under the disbonded coating of pipeline steel in near-neutral pH environment. Corros Sci 2010; 52: 3750–3756.

Eslami A, Kania R, Worthingham B, BovenG, Eadie R, Chen W. Effect of CO_2 and R-ratio on near-neutral pH stress corrosion cracking initiation under a disbonded coating of pipeline steel. Corros Sci 2011; 53: 2318–2327.

Gray L, Anderson B, Danysh M, Tremaine P. Mechanisms of carbon steel corrosion in brines containing dissolved carbon dioxide. In Proceedings of CORROSION/89 (CD. paper no. 464). Houston, TX: NACE, 1989.

Gray L, Anderson B, Danysh M, Tremaine P. Effect of pH and temperature on the mechanism of carbon steel corrosion by aqueous carbon dioxide. In Proceedings of CORROSION/90 (CD paper no. 40). Houston (TX): NACE, 1990.

Gu B, Luo J, Mao X. Hydrogen-facilitated anodic dissolution-type stress corrosion cracking of pipeline steels in near-neutral ph solution. Corrosion 1999; 55: 96–106.

Han J, Nešić S, Yang Y, Brown B. Spontaneous passivation observations during scale formation on mild steel in CO_2 brines. Electrochim Acta 2011; 55: 5396–5404.

Liu X, Mao X. Electrochemical polarization and stress corrosion cracking behaviours of a pipeline steel in dilute bicarbonate solution with chloride ion. Scr Metall Mater 1995; 33: 145–150.

Liu Z, Li X, Cheng Y. Mechanistic aspect of near-neutral pH stress corrosion cracking of pipelines under cathodic polarization. Corros Sci 2012; 55: 54–60.

Lu B, Luo J, Norton P, Ma H. Effects of dissolved hydrogen and elastic and plastic deformation on active dissolution of pipeline steel in anaerobic groundwater of near-neutral pH. Acta Mater 2009; 57: 41–49.

Lu B, Luo J, Norton P. Environmentally assisted cracking mechanism of pipeline steel in near-neutral pH groundwater. Corros Sci 2010; 52: 1787–1795.

Manfredi C, Otegui J. Failures by SCC in buried pipelines. Eng Failure Anal 2002; 9: 495–509.

Mao S, Gu B, Wu N, Qiao L. The mechanism of hydrogen-facilitated anodic-dissolution-type stress corrosion cracking: theories and experiments. Philos Mag A 2001; 21: 1813–1831.

Marchesani F, Donati E, Spinelli CM, Mannucci G, Demofonti G, Cabrini M, Pastore T, The Tap Project. In Proceedings of 1st International Conference “Super High Strength Steels”. Rome: AIM (CD), 2005.

National Energy Board. Report of Public Inquiry Concerning Stress Corrosion Cracking on Canadian Oil and Gas Pipelines. MH-2-95, 1996.

Nešić S, Postlethwaite J, Olsen S. An electrochemical model for prediction of corrosion of mild steel in aqueous carbon dioxide solutions. 1996a; 52: 280–294.

Nešić S, Thevenot N, Crolet J, Drazic D. Electrochemical properties of iron dissolution in the presence of CO_2 - basics revisited. In Proceedings of CORROSION/96 (CD Paper no. 3), Houston (TX): NACE, 1996b.

Niu L, Cheng Y. Corrosion behavior of X-70 pipe steel in near-neutral pH solution. Appl Surf Sci 2007; 253: 8626–8631.

Nordsveen M, Nešić S, Nyborg R, Stangeland A. A mechanistic model for carbon dioxide corrosion of mild steel in the presence of protective iron carbonate films – Part 1: theory and verification. Corrosion 2003; 59: 443–456.

Ogundele G, White W. Observations on the influences of dissolved hydrocarbon gases and variable water chemistries on corrosion of an API-L80 steel. Corrosion 1987; 3: 665–673.

Parkins RN. A review of stress corrosion cracking of high pressure gas pipelines. Proceedings of CORROSION/2000 (CD. paper 00363). Houston (TX): NACE, 2000.

Parkins RN, Fessler R. Stress corrosion cracking of high-pressure gas transmission pipelines. Int J Mater Eng Appl 1978; 1: 80–96.

Parkins RN, Zhou S. The stress corrosion cracking of C-Mn steel in CO_2-HCO_3^-, CO_3^{2-} solutions. II: electrochemical and other data. Corros Sci 1997; 39: 175–191.

Parkins RN, O’dell C, Fessler R. Factors affecting the potential of galvanostatically polarised pipeline steel in relation to SCC in CO_3^{2-}/HCO_3^- solutions. Corros Sci 1984; 24: 343–374.

Parkins RN, Belhimer E, Blanchard Jr W. Stress corrosion cracking characteristics of a range of pipeline steels in carbonate-bicarbonate solution. Corrosion 1993; 49: 951–966.

Parkins RN, Blanchard W, Delanty B. Transgranular stress corrosion cracking of high-pressure pipelines in contact with solutions of near neutral pH. Corrosion 1994; 50: 394–408.

Punter A, Fikkers A, Vanstaen G. Hydrogen-induced stress corrosion cracking on a pipeline. Mater Performance 1992; 31: 24–28.

Riley A, Sykes J. The active-passive transition in low alloy steels in carbonate solutions. Electrochim Acta 1990; 35: 35–45.

Shipilov A, May I. Structural integrity of aging buried pipelines having cathodic protection. Eng. Failure Anal 2006; 13: 1159–1176.

Sinigaglia E, Cabrini M. Electrochemical and stress corrosion cracking behaviour of micro-alloyed steels in CO_2/HCO_3^- environment. Proceedings of CORROSION/97. San Diego Houston (TX): NACE, 1997.

Spinelli CM, Marchersani F. TAP Project. 2004 In Proceedings of International Pipeline Conference, pp. 757–762. Calgary, Alberta, Canada (CD), 2004.

Van Boven G, Chen W, Rogge R. The role of residual stress in neutral pH stress corrosion cracking of pipeline steels. Part I: pitting and cracking occurrence. Acta Mater 2007; 55: 29–42.

Wieckowski A, Ghali E, Szklarczyk M, Sobkowski J. The behaviour of iron electrode in CO_2 - saturated neutral electrolyte- I electrochemical study. Electrochim Acta 1983; 28: 1619–1626.

Xing X, ChenW, Zhang H. Prediction of crack propagation under cyclic loading based on hydrogen diffusion. Mater Lett 2015; 152: 86–89.

Yu M, Xing X, Zhang H, Zhao J, EadieR, Chen W, Kania R. Corrosion fatigue crack growth behavior of pipeline steel under underload-type variable amplitude loading schemes. Acta Mater 2015; 96: 159–169.

Zhao J, Chevil K, Yu M, Been J. Statistical analysis on underload-type pipeline spectra. J Pipeline System Eng Practice 2016; 7: 1–1.

Zhao J, Chen W, Yu M, Chevil K, Eadie R, Been J, Keane S. Crack growth modeling and life prediction of pipeline steels exposed to near-neutral pH environments: stage II crack growth and overall life prediction. Metall Mater Trans A 2017a; 48: 1641–1652.

Zhao J, Chen W, Yu M, Chevil K, Eadie R, Van Boven G, Keane S. Crack growth modeling and life prediction of pipeline steels exposed to near-neutral pH environments: dissolution crack growth and occurrence of crack dormancy in stage I. Metall Mater Trans A 2017b; 48: 1629–1640.